Electronic Supplementary Information (ESI)

Multi-stimuli-responsive luminescence enabled by crown ether anchored chiral antimony halide phosphors

Xiao Han, [a] *Puxin Cheng,* [a] *Shanshan Han,* [a] *Junjie Guan,* [a] *Zhihua Wang,* [a] *Wenqing Han,* [a] *Rongchao Shi,* [a] *Songhua Chen,* [b] *Yongshen Zheng,* *[a] *Jialiang Xu*[a] *and Xian-He Bu* [a]

[a] School of Materials Science and Engineering, Smart Sensing Interdisciplinary Science Center, Frontiers Science Center for New Organic Matter, Nankai University, Tongyan Road 38, Tianjin 300350, P. R. China

E-mails: yszheng@nankai.edu.cn; jialiang.xu@nankai.edu.cn.

[b] College of Chemistry and Material Science, Longyan University, Longyan 364012, Fujian, P.R. China.

Supplementary Figures

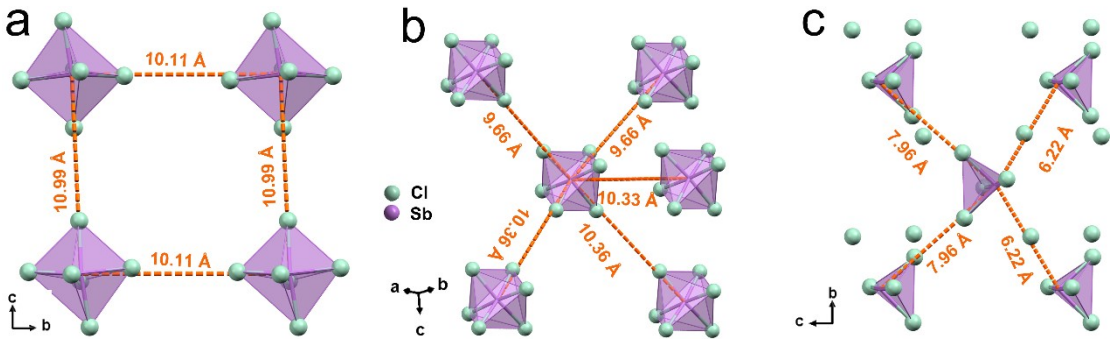

Fig. S1 The closest neighboring Sb···Sb distances (orange dotted lines) in the (a) ***R*-Sb**, (b) ***rac*-Sb**, and (c) ***S*-PPD-Sb** crystals.

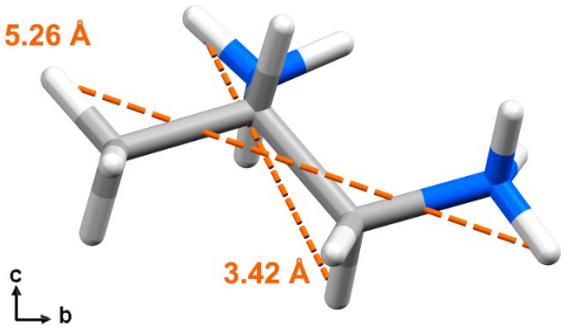

Fig. S2 The size of [*S*-PPD]$^{2+}$ cation in the ***S*-PPD-Sb** crystal.

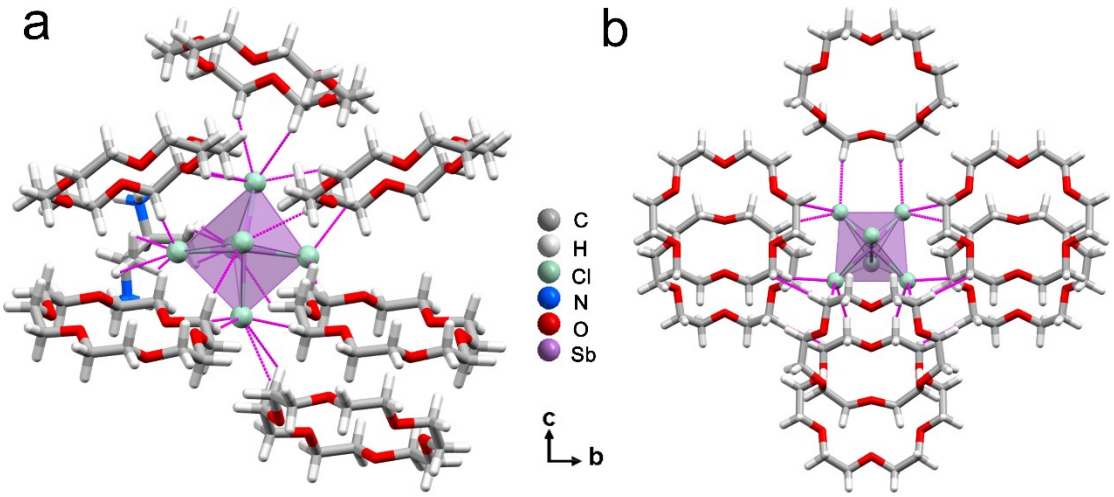

Fig. S3 Sb–Cl···H–C hydrogen bonding interactions (magenta dotted lines) viewed along a-axis in (a) ***R*-Sb** and (b) ***rac*-Sb**.

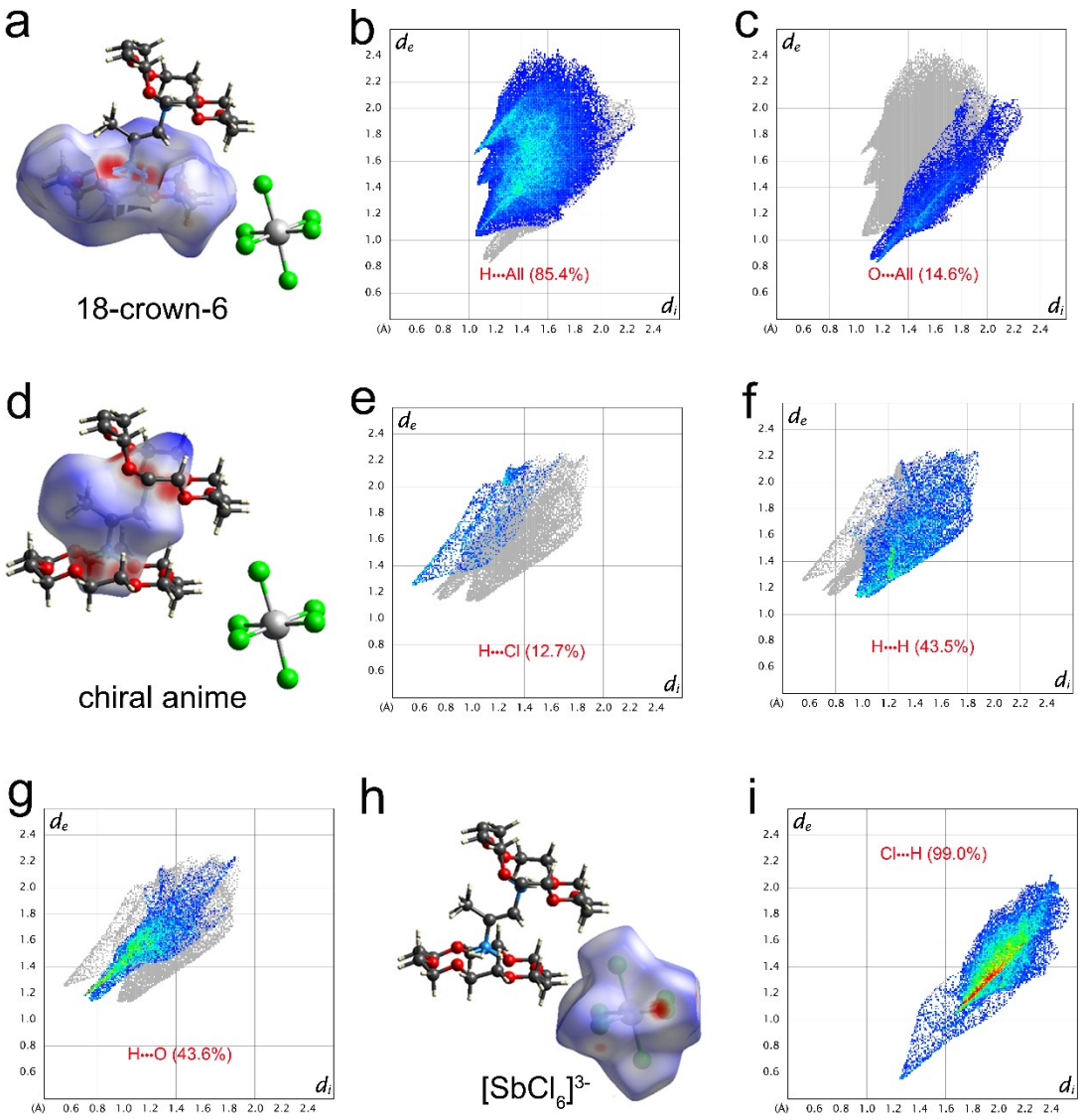

Fig. S4 Hirshfeld d_{norm} surfaces of (a) 18-crown-6, and the corresponding 2D fingerprint plots for (b) H···All and (c) O···All in ***R*-Sb**; Hirshfeld d_{norm} surfaces of (d) chiral 1,2-propanediamine cation, and the corresponding 2D fingerprint plots for (e) H···Cl , (f) H···H and (g) H···O in ***R*-Sb**; and (h) Hirshfeld d_{norm} surfaces of $[SbCl_6]^{3-}$ octahedron in ***R*-Sb**, and the corresponding 2D fingerprint plots for (i) Cl···H.

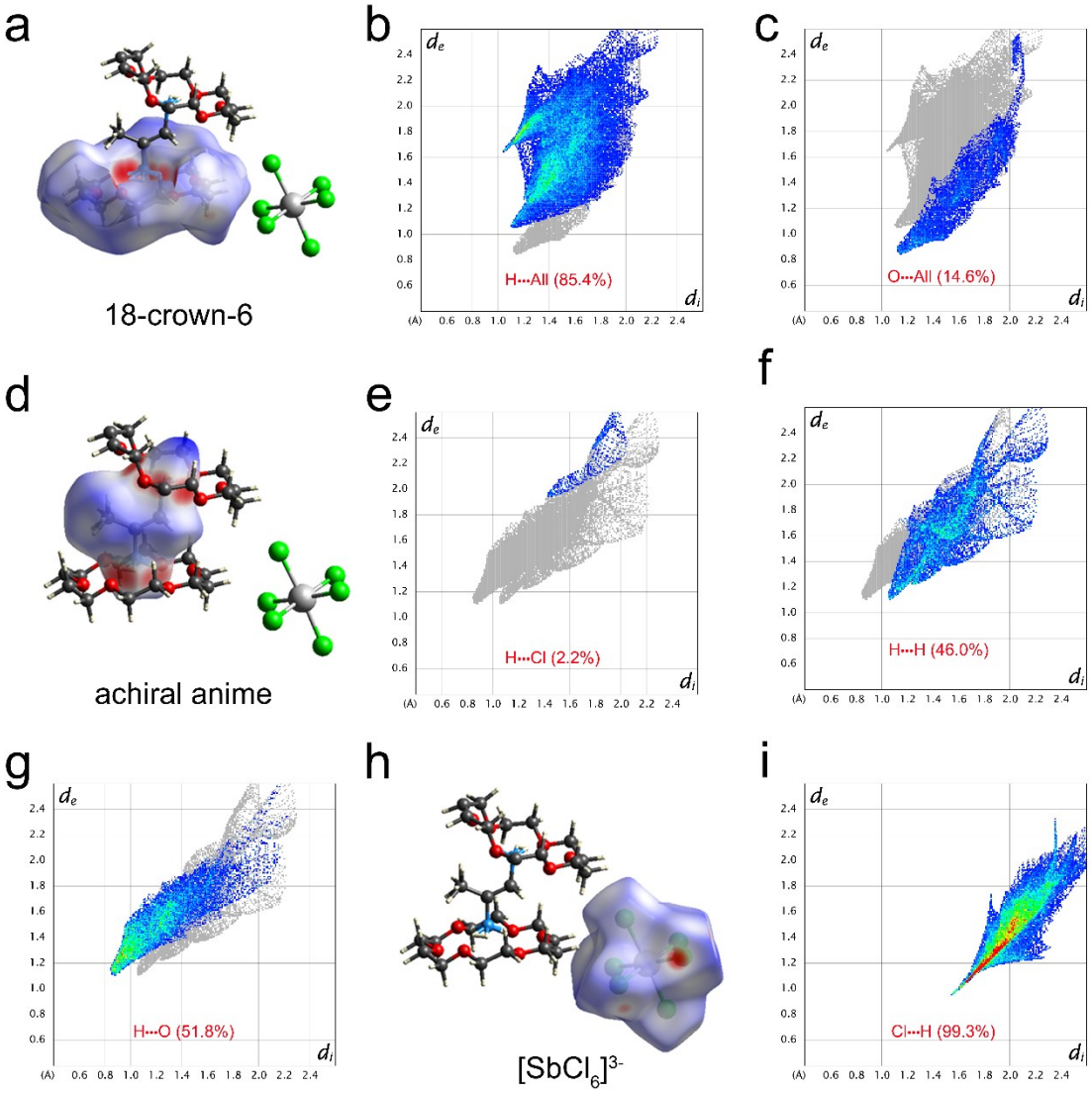

Fig. S5 Hirshfeld d_{norm} surfaces of (a) 18-crown-6, and the corresponding 2D fingerprint plots for (b) H···All and (c) O···All in ***rac*-Sb**; Hirshfeld d_{norm} surfaces of (d) achiral 1,2-propanediamine cation, and the corresponding 2D fingerprint plots for (e) H···Cl , (f) H···H and (g) H···O in ***rac*-Sb**; and (h) Hirshfeld d_{norm} surfaces of $[SbCl_6]^{3-}$ octahedron in ***rac*-Sb**, and the corresponding 2D fingerprint plots for (i) Cl···H.

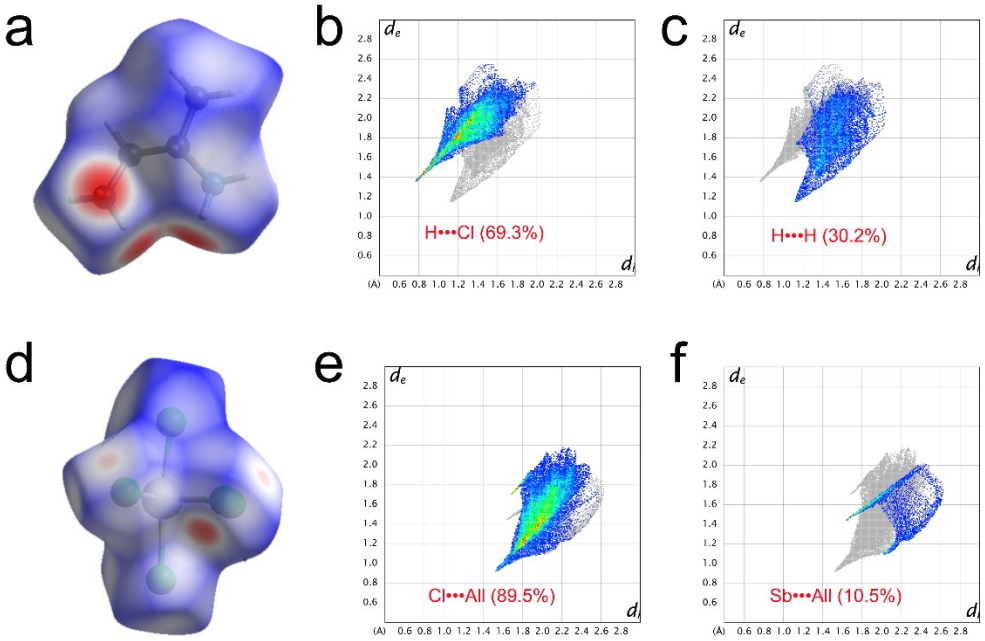

Fig. S6 Hirshfeld d_{norm} surfaces of (a) chiral $[S\text{-PPD}]^{2+}$ cation, and the corresponding 2D fingerprint plots for (b) H···Cl and (c) H···H in ***S*-PPD-Sb**; Hirshfeld d_{norm} surfaces of (d) $[SbCl_4Cl]^{2-}$ polyhedrons, and the corresponding 2D fingerprint plots for (e) Cl···All, (f) Sb···All.

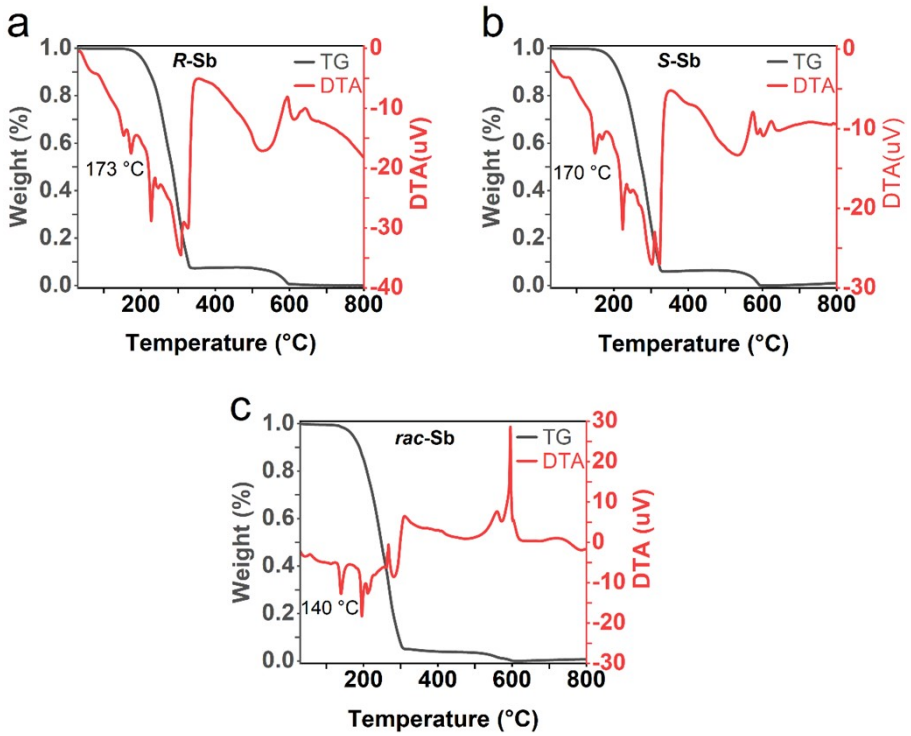

Fig. S7 TG–DTA analysis of (a) ***R*-Sb**, (b) ***S*-Sb** and (c) ***rac*-Sb**.

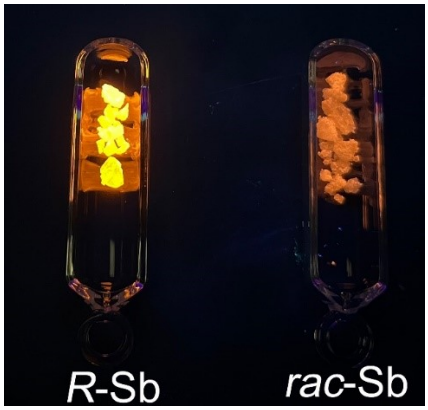

Fig. S8 PL images of ***R*-Sb** and ***rac*-Sb** under the radiation of 365 nm UV.

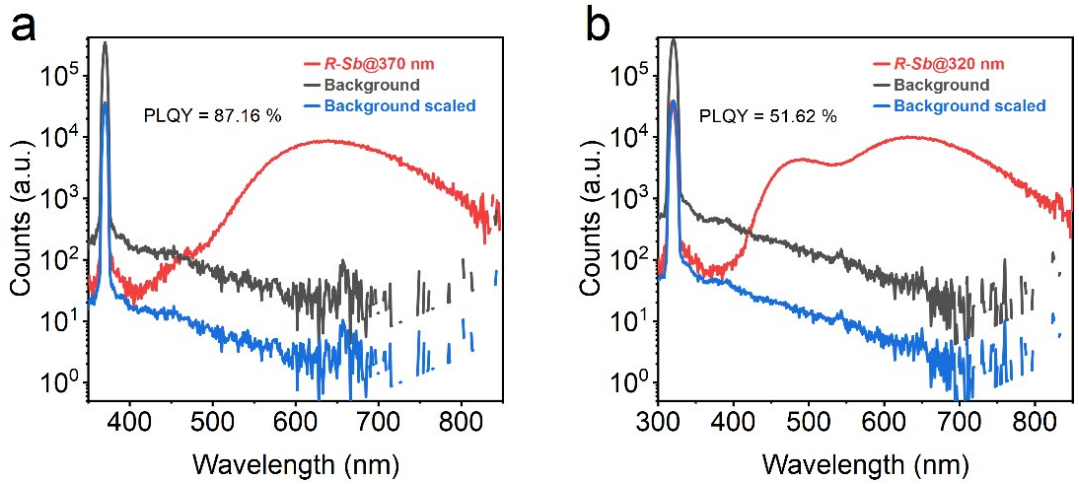

Fig. S9 Photoluminescence quantum yield of ***R*-Sb** at excitation of (a) 370 nm and (b) 320 nm.

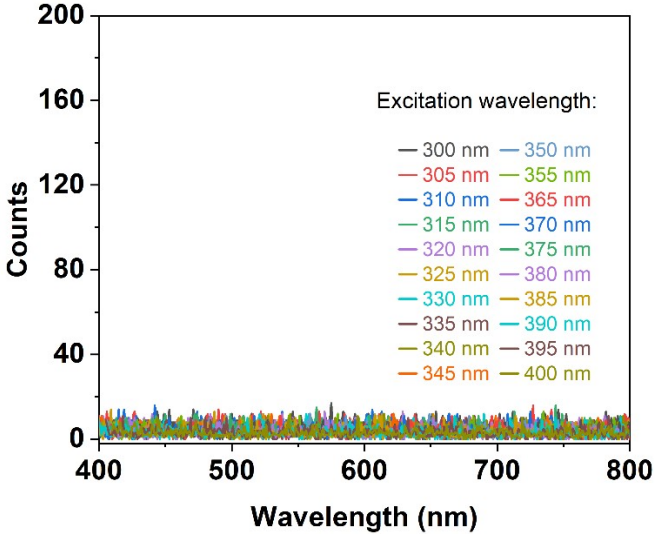

Fig. S10 Excitation-emission mapping patterns of ***S*-PPD-Sb**.

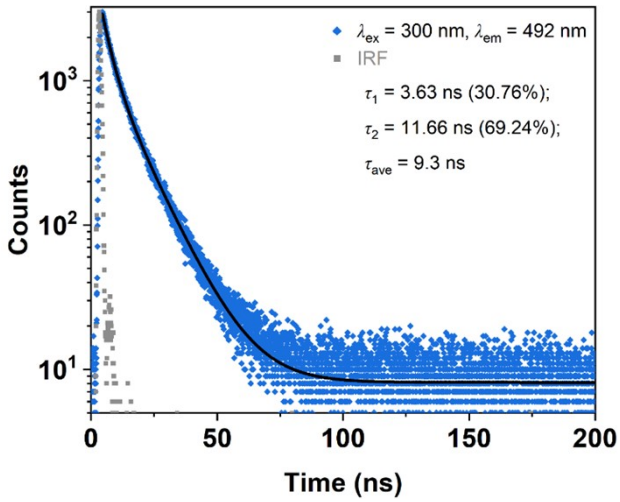

Fig. S11 Time-resolved PL decay spectrum of ***R*-Sb** at 492 nm.

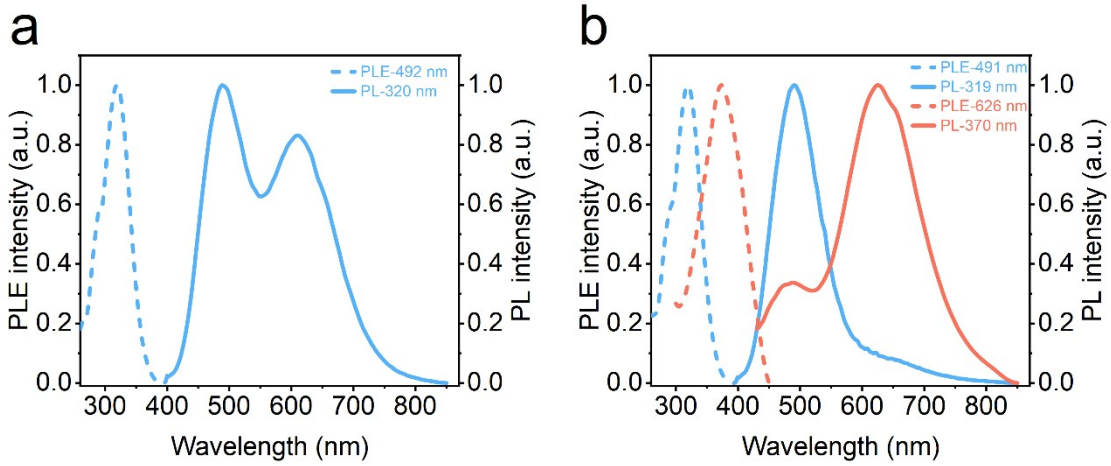

Fig. S12 PL and PLE spectra for (a) ***R*-Sb** and (b) ***rac*-Sb**.

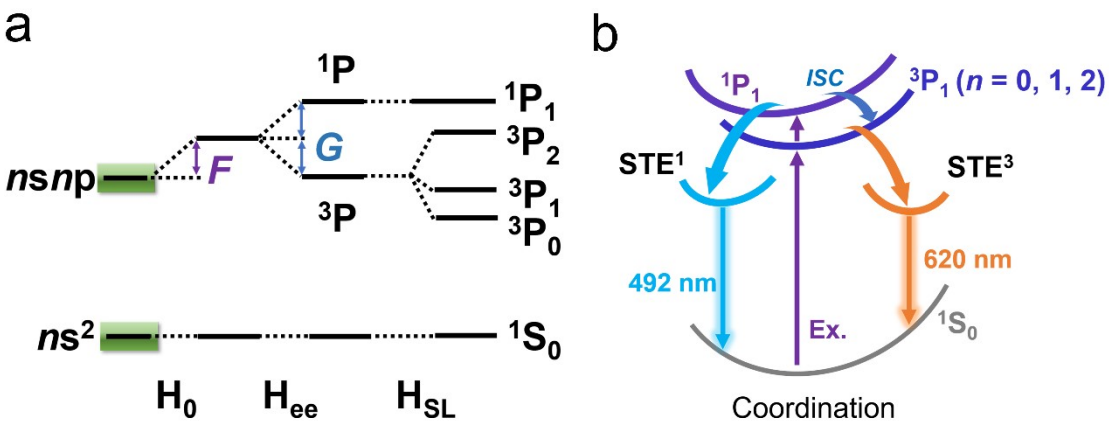

Fig. S13 (a) Energy level diagram for the ns^2 ground-state configuration. *F* and *G* represent Coulomb and exchange interactions, respectively. (b) Schematic diagram of the energy level structure of photoluminescence in ***R*-Sb**.

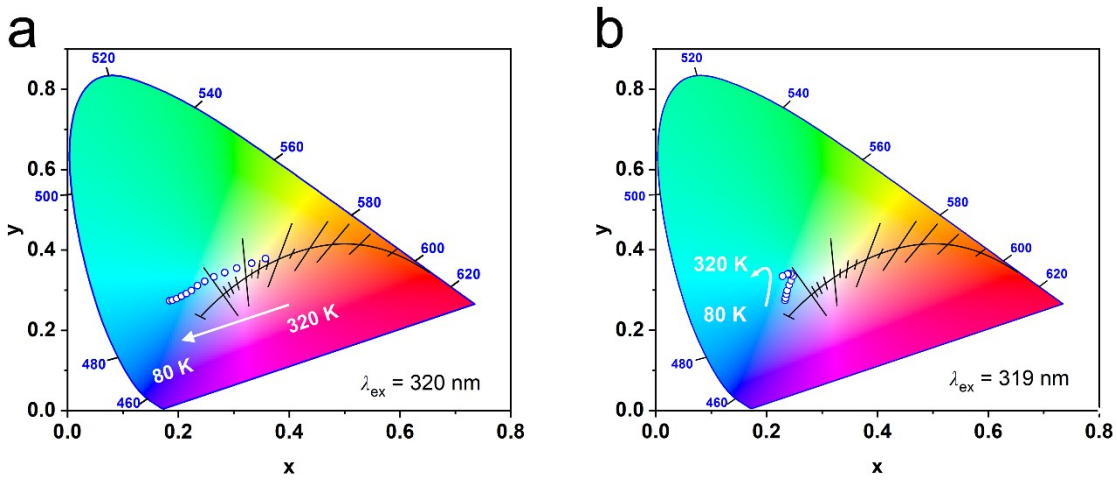

Fig. S14 The Commission Internationale de l'Eclairage (CIE) chromaticity coordinates at different temperature for (a) ***R*-Sb** and (b) ***rac*-Sb**.

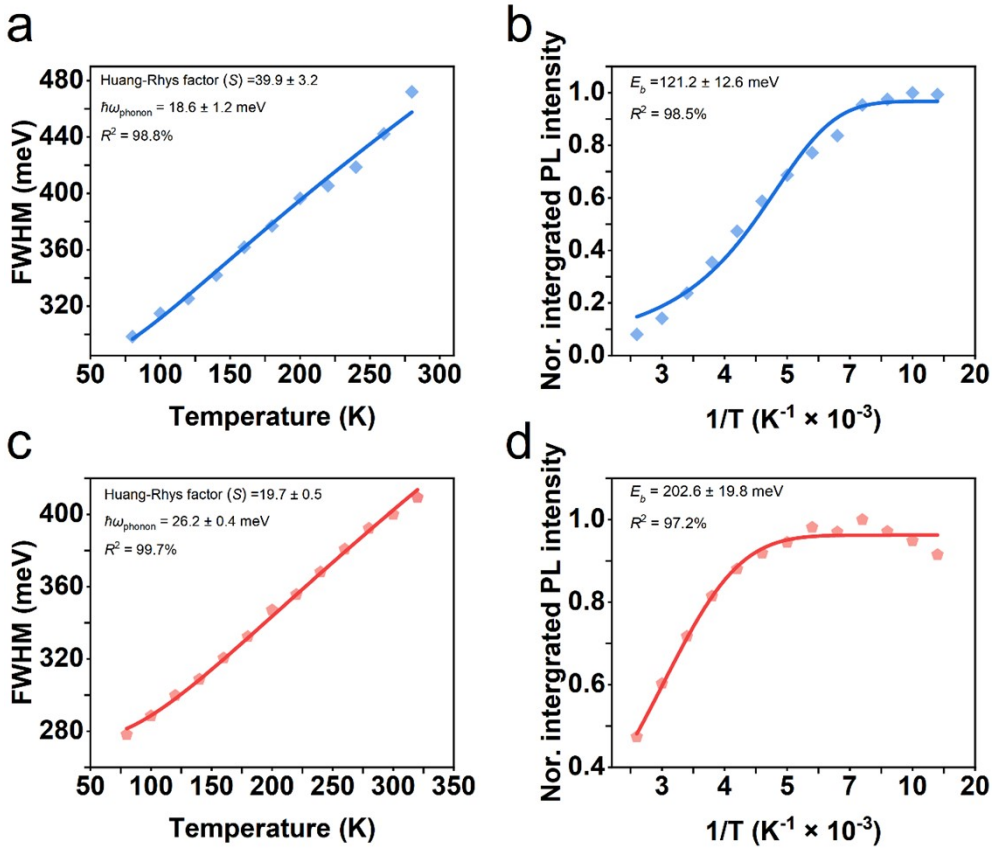

Fig. S15 (a) FWHM and (b) integrated PL intensity of 492 nm as a function of temperature for ***R*-Sb**; (c) FWHM and (d) integrated PL intensity of 612 nm as a function of temperature for ***R*-Sb**.

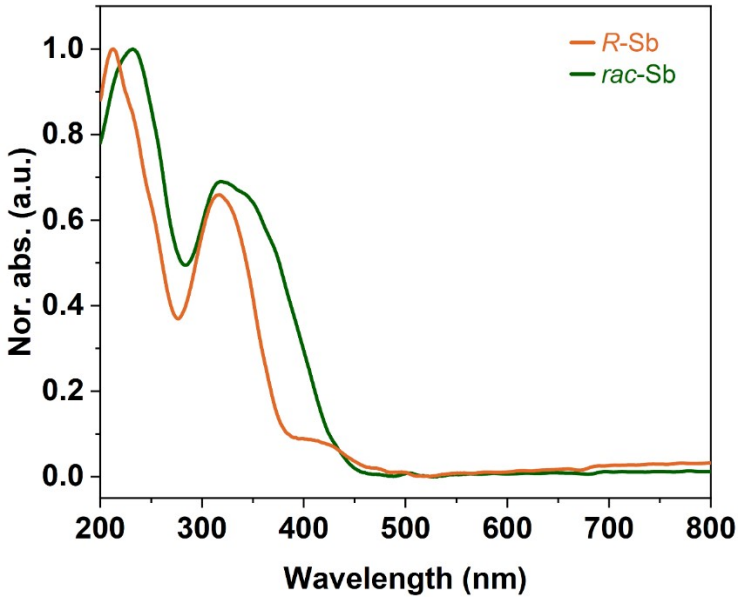

Fig. S16 Normalized UV–vis absorption spectra of ***R*-Sb** and ***rac*-Sb**.

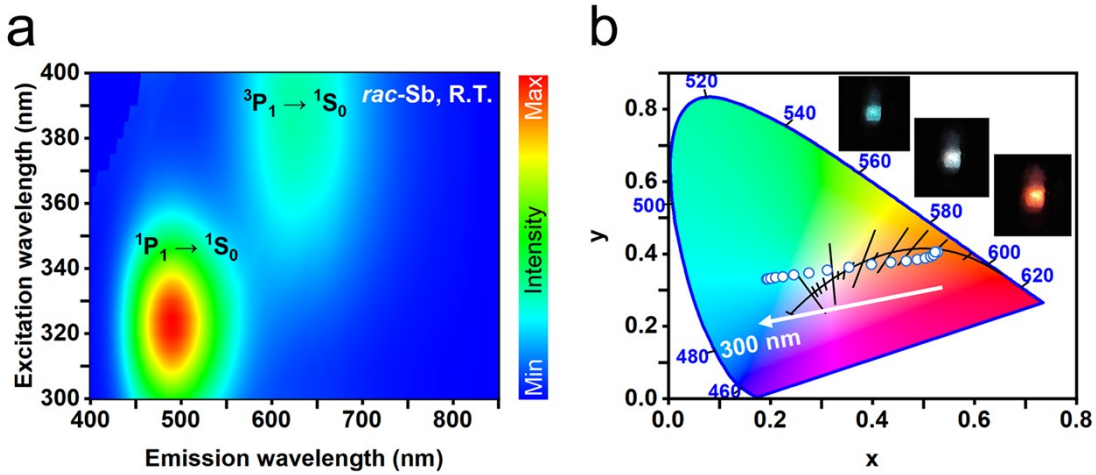

Fig. S17 (a) Excitation-emission mapping patterns of ***rac*-Sb** at ambient. (b) The corresponding CIE chromaticity coordinates at different excitation wavelengths. Inset: luminescent photographs at excitation of 320 nm (left), 335 nm (medium), and 370 nm (right).

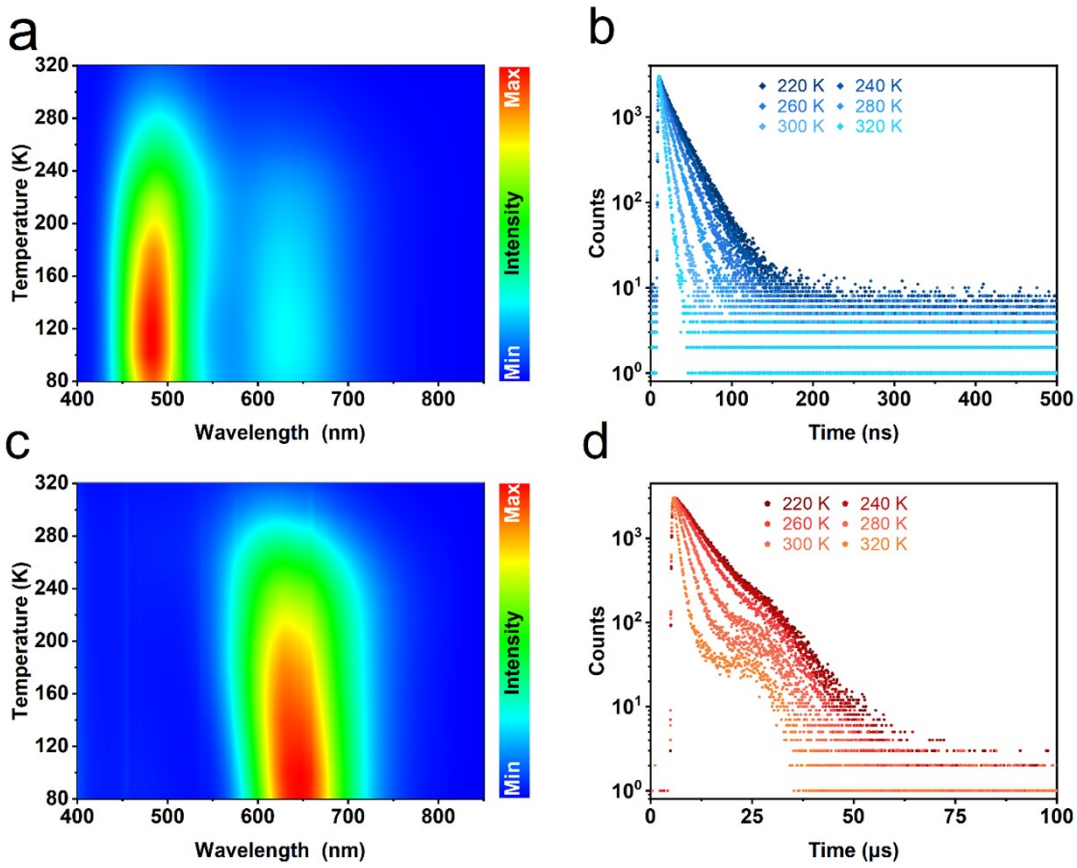

Fig. S18 (a) Temperature-dependent PL spectra (λ_{ex} = 319 nm) and (b) decay PL spectra (λ_{ex} = 300 nm) for ***rac*-Sb**; (c) temperature-dependent PL spectra (λ_{ex} = 371 nm) and (b) decay PL spectra (λ_{ex} = 371 nm) for ***rac*-Sb**.

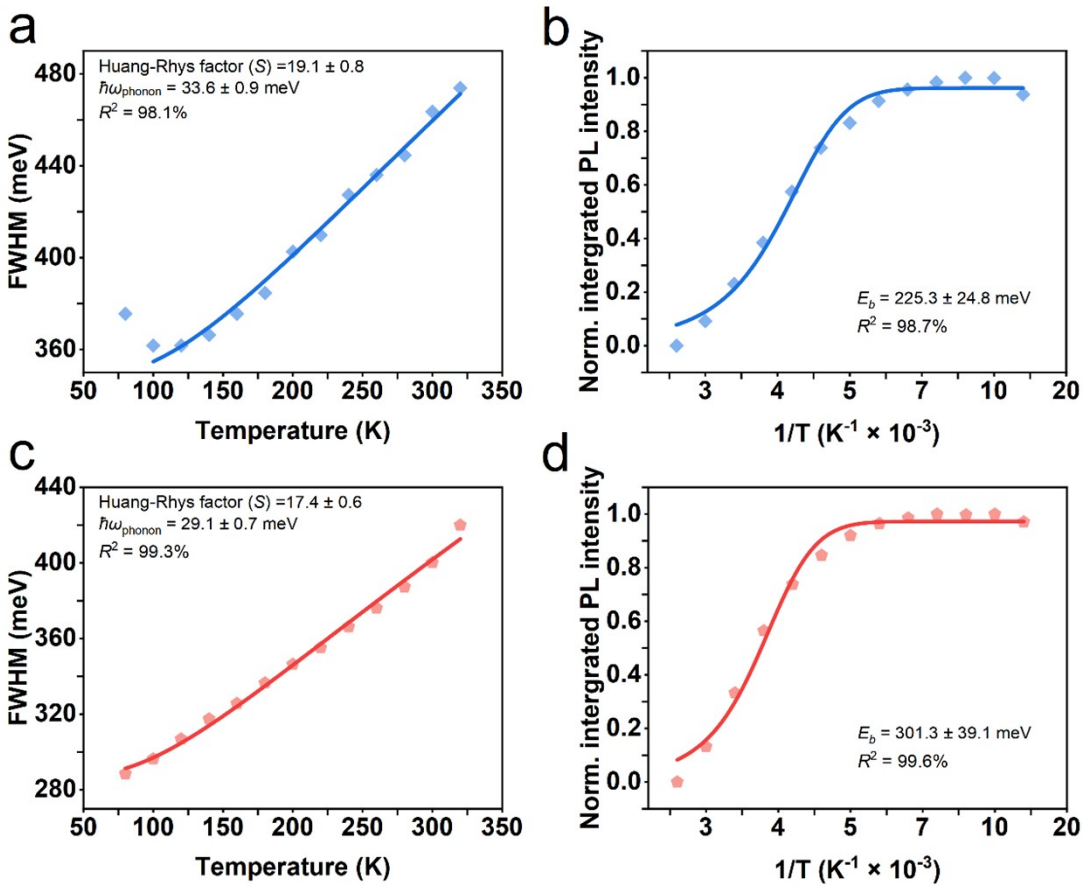

Fig. S19 (a) FWHM and (b) integrated PL intensity of 491 nm as a function of temperature for ***rac*-Sb**; (c) FWHM and (d) integrated PL intensity of 626 nm as a function of temperature for ***rac*-Sb**.

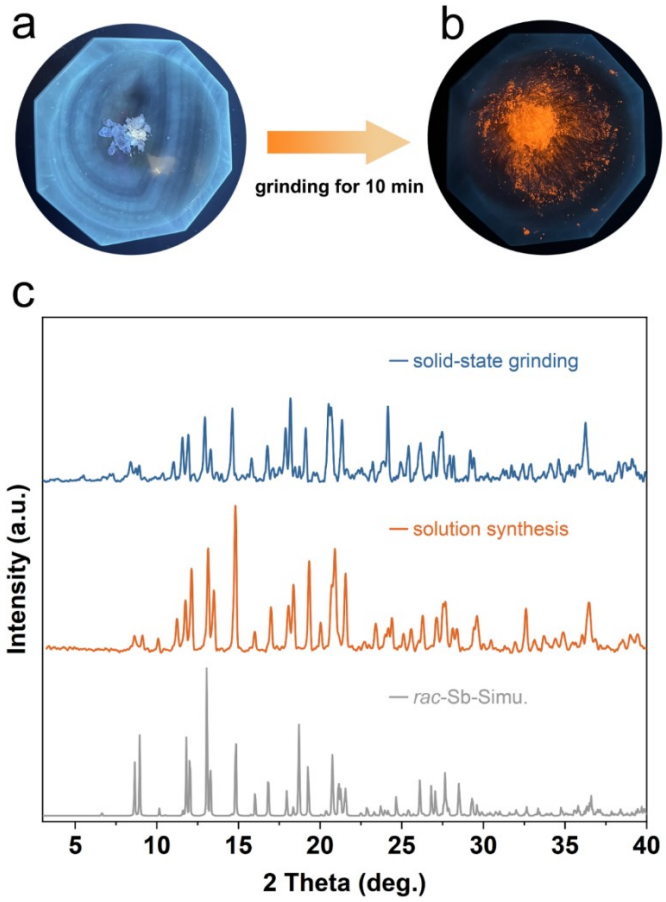

Fig. S20 Solid-state synthesis of ***rac*-Sb**. Images of the sample before (a) and after (b) mechanical grinding under 365 nm UV lamp. (c) XRD patterns of ***rac*-Sb** prepared by solid-state grind and solution synthesis.

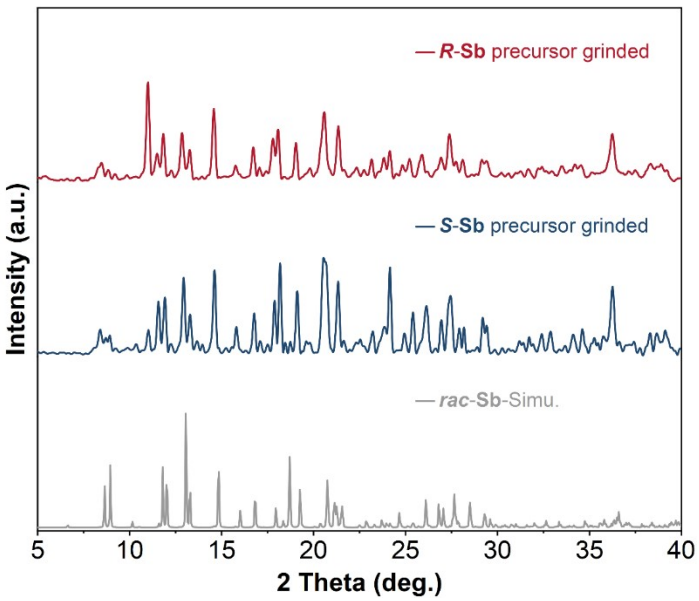

Fig. S21 XRD patterns of the samples prepared by solid-state grinding the ***R*-Sb** and ***S*-Sb** precursor materials.

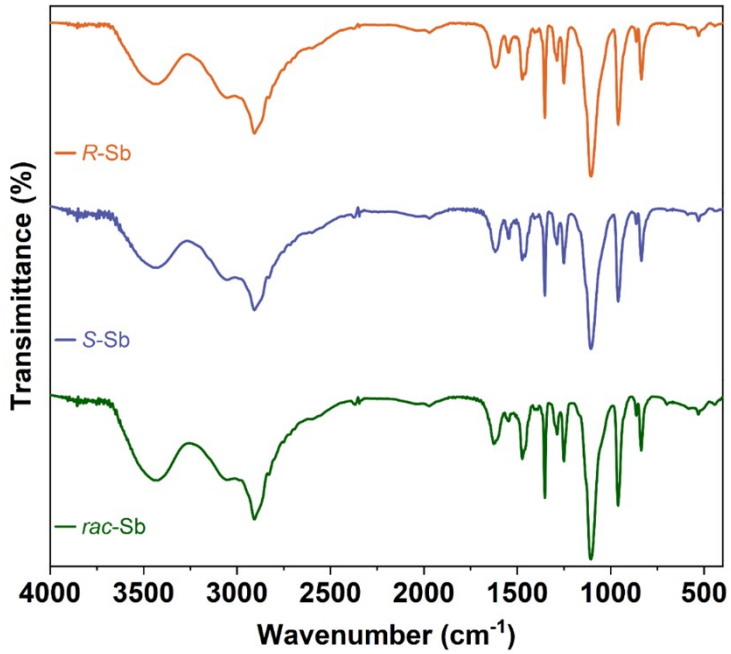

Fig. S22 FT-IR spectra of ***R*-Sb**, ***S*-Sb** and ***rac*-Sb**.

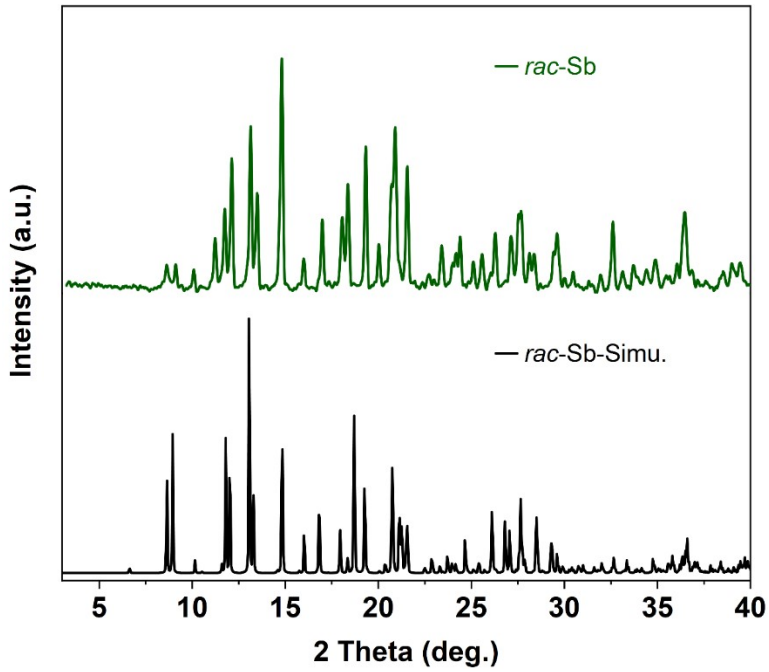

Fig. S23 PXRD patterns of ***rac*-Sb**, including experimental powder diffraction data (red line) and simulated data (black line).

Supplementary Tables

Table. S1 Crystallographic data and refinement details for ***R*-Sb**, ***S*-Sb** and ***rac*-Sb**.

Identification code	***R*-Sb**	***S*-Sb**	***rac*-Sb**
Empirical formula	$C_{27}H_{60}Cl_6N_2O_{12}Sb$	$C_{27}H_{60}Cl_6N_2O_{12}Sb$	$C_{27}H_{60}Cl_6N_2O_{12}Sb$
Formula weight	939.22	939.22	939.22
Temperature/K	100	100	100
Crystal system	tetragonal	tetragonal	monoclinic
Space group	$P4_32_12$	$P4_12_12$	$P2_1/m$
a/Å	10.11990(10)	10.11536(4)	10.3335(2)
b/Å	10.11990(10)	10.11536(4)	14.7221(4)
c/Å	38.9943(4)	38.9841(2)	13.4584(4)
α/°	90	90	90
β/°	90	90	97.826(2)
γ/°	90	90	90
Volume/Å^3	3993.50(9)	3988.87(4)	2028.37(9)
Z	4	4	2
ρ_{calc} g/cm^3	1.562	1.564	1.538
μ/mm^{-1}	9.656	9.667	1.130
F(000)	1940.0	1940.0	970.0
Reflections collected	23730	26882	28768
Data/restraints/parameters	4107/0/224	4115/121/234	5617/126/238
Goodness-of-fit on F^2	1.075	1.058	1.051
Final R indexes [I>=2σ (I)]	R_1 = 0.0639, wR_2 = 0.1861	R_1= 0.0652, wR_2= 0.1762	R_1= 0.1023, wR_2= 0.2833
Final R indexes [all data]	R_1= 0.0652, wR_2= 0.1875	R_1= 0.0660, wR_2= 0.1770	R_1= 0.1118, wR_2 = 0.2917
CCDC	2303422	2303423	2303424

Table. S2 Selected bond lengths (Å) for for ***R*-Sb**, ***S*-Sb** and ***rac*-Sb**.

***R*-Sb**		***S*-Sb**		***rac*-Sb**	
Sb1-Cl1	2.600(2)	Sb1-Cl2[b]	2.600(2)	Sb1-Cl4	2.620(2)
Sb1-Cl1[a]	2.600(2)	Sb1-Cl2	2.599(2)	Sb1-Cl2	2.595(2)
Sb1-Cl2[a]	2.468(4)	Sb1-Cl1	2.470(3)	Sb1-Cl1	2.483(4)
Sb1-Cl2	2.468(4)	Sb1-Cl1[b]	2.470(3)	Sb1-Cl1[c]	2.483(4)
Sb1-Cl3[a]	2.580(4)	Sb1-Cl3[b]	2.576(4)	Sb1-Cl3	2.420(3)
Sb1-Cl3	2.580(4)	Sb1-Cl3	2.576(4)	Sb1-Cl3[c]	2.420(3)
C1-C1[a]	1.523(15)	C15-C14	1.53(5)	N1-C2	1.493(13)
C1-C2	1.51(2)	N2-C13	1.50(4)	O1-C4[c]	1.415(9)
N1-C1	1.485(10)	C13-C14	1.515(16)	O1-C4	1.415(9)
O6-O13	1.426(11)	O1-C1	1.41611)	O2-C5	1.393(11)

[a)] 1-Y,1-X,3/2-Z; [b)] -1+Y,1+X,1-Z; [c)] +X,1/2-Y,+Z

Table. S3 Selected bond angles (°) for ***R*-Sb**, ***S*-Sb** and ***rac*-Sb**.

***R*-Sb**		***S*-Sb**		***rac*-Sb**	
Cl1-Sb1-Cl1[a]	169.94(11)	Cl2-Sb1-Cl2[b]	169.94(11)	Cl2-Sb1-Cl4	176.45(10)
Cl2-Sb1-Cl1	87.27(7)	Cl1[b] -Sb1-Cl2	87.21(7)	Cl1[a]-Sb1-Cl4	87.22(7)
Cl2[a]-Sb1-Cl1	85.87(7)	Cl1[b]-Sb1-Cl2[b]	85.91(7)	Cl1-Sb1-Cl4	87.22(7)
Cl2 -Sb1-Cl1[a]	85.86(7)	Cl1-Sb1-Cl2[b]	87.22(7)	Cl1[a]-Sb1-Cl2	90.37(9)
Cl2[a]-Sb1-Cl1	87.27(7)	Cl-Sb1-Cl2	85.91(7)	Cl1-Sb1-Cl2	90.37(9)
Cl2-Sb1-Cl2[a]	93.89(12)	Cl1[b]-Sb1-Cl3	93.74(12)	Cl1[a]-Sb1-Cl1	94.25(18)
Cl2-Sb1-Cl3[a]	166.29(11)	Cl1[b]-Sb1-Cl3[b]	98.08(10)	Cl3[a]-Sb1-Cl4	92.62(9)
Cl2-Sb1-Cl3	97.93(11)	Cl1-Sb1-Cl3	98.08(10)	Cl3-Sb1-Cl4	92.62(9)
Cl2[a]-Sb1-Cl3[a]	97.93(11)	Cl1[b] -Sb1-Cl3	166.25(10)	Cl3[a]-Sb1-Cl2	90.08(11)
Cl2[a]-Sb1-Cl3	166.29(11)	Cl1-Sb1-Cl3[b]	166.25(10)	Cl3-Sb1-Cl2	90.08(11)
Cl3[a]-Sb1-Cl1[a]	87.79(11)	Cl3[b] -Sb1-Cl2[b]	100.57(10)	Cl3[a]-Sb1-Cl1[a]	173.46(13)
Cl3[a]-Sb1-Cl1	100.43(10)	Cl3-Sb1-Cl2	100.57(10)	Cl3-Sb1-Cl1[a]	92.25(15)
Cl3[a] -Sb1-Cl1	100.43(10)	Cl3-Sb1-Cl2[b]	87.67(10)	Cl3-Sb1-Cl1	173.46(13)
Cl3-Sb1-Cl1	87.79(11)	Cl3[b]-Sb1-Cl2	87.66(10)	Cl3[a]-Sb1-Cl1	92.25(15)
Cl3-Sb1-Cl3	71.23(19)	Cl3[b] -Sb1-Cl3	71.18(18)	Cl3-Sb1-Cl3[a]	81.2(2)
C13-O6-C12	111.7(7)	N2-C13-C14	110(2)	C1-C2-N1	115.1(10)
C14-O1-C3	111.7(7)	N1-C13-C13[b]	111.2(8)	C3-C2-N1	114.2(11)
C10-O5-C11	111.3(7)	C13-C14-C15	120(2)	C3-C2-C1	130.7(12)
C8-O4-C9	111.4(7)	N1-C14-C15	103(3)	C14-O6-C13	109.4(6)
C6-O3-C7	104.4(10)	N1-C14-C13	111(2)	C15[a]-O5-C15	108.3(13)
C4-O2-C5	107.4(8)	C6-O4-C7	105.2(10)	O2-C6-C7	126.7(18)
N1-C1-C1[a]	110.8(8)	C8-O5-C9	111.6(7)	O3-C7-C6	110.9(8)
N1-C1-C2	105.9(9)	C10-O6-C11	111.5(7)	O4-C9-C8	107.7(10)

[a)] 1-Y,1-X,3/2-Z; [b)] -1+Y,1+X,1-Z; [c)] +X,1/2-Y,+Z

Table. S4 Crystallographic data and refinement details for ***S*-PPD-Sb**.

Identification code	***S*-PPD-Sb**
Empirical formula	$C_6H_{24}Cl_7N_4Sb$
Formula weight	522.19
Temperature/K	100.00(10)
Crystal system	orthorhombic
Space group	$P2_12_12_1$
a/Å	9.16220(10)
b/Å	10.5718(2)
c/Å	19.3536(4)
α/°	90
β/°	90
γ/°	90
Volume/Å^3	1874.61(6)
Z	4
ρ_{calc} g/cm^3	1.850
μ/mm^{-1}	2.460
F(000)	1032.0
Reflections collected	18707
Data/restraints/parameters	4998/0/169
Goodness-of-fit on F^2	1.046
Final R indexes [I>=2σ (I)]	R_1 = 0.0135, wR_2 = 0.0288
Final R indexes [all data]	R_1 = 0.0139, wR_2 = 0.0289
CCDC	2303425

Table. S5 Selected bond lengths (Å) for for ***S*-PPD-Sb**.

***S*-PPD-Sb**	
Sb1-Cl5	2.4149(5)
Sb1-Cl6	2.6827(5)
Sb1-Cl7	2.4355(5)
Sb1-Cl4	2.5226(5)
N3-C4	1.491(3)
N1-C2	1.502(2)
N2-C3	1.492(3)
N4-C6	1.510(3)
C3-C2	1.527(3)
C2-C1	1.520(3)

Table. S6 Selected bond angles (˚) for ***S*-PPD-Sb**.

***S*-PPD-Sb**	
Cl5-Sb1-Cl6	88.798(17)
Cl5-Sb1-Cl7	87.232(15)
Cl5-Sb1-Cl4	91.794(18)
Cl7-Sb1-Cl6	85.767(16)
Cl7-Sb1-Cl4	88.458(17)
Cl4-Sb1-Cl6	174.160(17)
N2-C3-C2	109.77(16)
N1-C2-C3	107.44(16)
N1-C2-C1	109.83(16)
C1-C2-C3	113.94(16)
N4-C6-C7	108.92(16)
N4-C6-C4	110.62(16)
C7-C6-C4	109.66(17)
N3-C4-C6	113.75(18)

Table. S7 Luminescence dissymmetry factors of various chiral antimony halides

Chiral HOMHs	Dimensionality	g_{lum}	PLQY[a)]	Reference
(*R*, *R*/*S*, *S*-DCDA)$_3$Sb$_2$Cl$_{12}$	0D	3.22 × 10^{-3}	27.6%	[1]
R-/*S*-(C$_5$H$_{12}$NO)$_2$SbCl$_5$	0D	1.2 × 10^{-3}	2.16%	[2]
(*R*/*S*)-C$_6$H$_{15}$Cl$_2$NO·SbCl$_5$	0D	2.5 × 10^{-4}	71.2%	[3]
***R*-/*S*-Sb**	0D	5.7 × 10^{-3}	87.16%	This work

[a)]The PLQY is the highest quantum yield among the various excitation wavelengths

Supplementary References

[1] C.-Y. Chai, X.-B. Han, C.-D. Liu, C.-C. Fan, B.-D. Liang, W. Zhang, *J. Phys. Chem. Lett.* **2023**, 14, 4063.

[2] D.-Y. Liu, H.-Y. Li, R.-P. Han, H.-L. Liu, S.-Q. Zang, *Angew. Chem. Int. Ed.* **2023**, 62, e202307875.

[3] H.-L. Xuan, J.-L. Li, L.-J. Xu, D.-S. Zheng, Z.-N. Chen, *Adv. Opt. Mater.* **2022**, 10, 2200591.